Spectral characterisation of hydrothermal alteration associated with sediment-hosted Cu-Ag mineralisation in the Central European Kupferschiefer

Léa Géring[1]*, Moritz Kirsch[1], Samuel Thiele[1], Andréa De Lima Ribeiro[1], Richard Gloaguen[1], Jens Gutzmer[1]

[1]Helmholtz-Zentrum Dresden-Rossendorf, Helmholtz Institute Freiberg for Resource Technology, 09599 Freiberg, Germany

Correspondence to: Léa Géring (lea.gering@hotmail.fr)

Abstract. The analysis of hydrothermal alteration in exploration drill cores allows to trace fluid-rock interaction processes, identify fluid flow paths and thus determine vectors in mineral systems. Hyperspectral imaging techniques are increasingly being employed to fill the scale gap between lab-based petrographic or geochemical analyses and the typical size of exploration targets. Hyperspectral imaging permits the rapid, cost-efficient and continuous characterisation of alteration mineralogy and texture along entire drill cores with a spatial sampling of a few millimetres. In this contribution, we present the results of an exploratory study on three mineralised drill cores from the Spremberg-Graustein Kupferschiefer-type Cu-Ag deposit in the Lusatia region of Germany. We demonstrate that hyperspectral imaging is a tool well-suited to recognize and track the effects of hydrothermal alteration associated with stratabound hydrothermal mineralization. Micro X-ray fluorescence spectrometry was used to validate the alteration mineral assemblages identified in hyperspectral data acquired in the visible, near, shortwave, mid-wave and long-wave infrared. Spectral features associated with the occurrence of iron oxide, kaolinite, sulphate, and carbonates were identified and mapped. We identify intensive hydrothermal alteration of the sandstones immediately below the Kupferschiefer horizon *sensu stricto*, spatially associated with or stratigraphically adjacent to Cu-Ag mineralisation. Importantly, we can clearly distinguish two mineralogically distinct styles of alteration (hematite and ferran carbonate) that bracket high-grade Cu-Ag mineralisation. The occurrence of well crystalline kaolinite in the sandstone units is spatially and genetically related to Cu-Ag mineralisation. Proximal Fe-carbonate and kaolinite alteration have not previously been documented for the high-grade Cu-Ag deposits of the Central European Kupferschiefer. Hematite alteration is well known in Kupferschiefer-type ore deposits. It marks the flow path of oxidising, metal-bearing hydrothermal fluids towards the site of hydrothermal sulphide mineralization. Ferran carbonate alteration in carbonate rocks located above the main mineralized zone, in contrast, is interpreted to mark hydrothermal fluid discharge from the mineralizing system. Although this study is limited to a small number of drill cores, our results suggest that hyperspectral imaging techniques may be used to identify vectors towards high-grade Cu-Ag mineralisation in Kupferschiefer-type mineral systems.

1. Introduction

The Central European Kupferschiefer is one of the largest and most prolific sediment-hosted copper districts globally (Borg et al., 2012). Economically important stratabound Cu-Ag mineralisation is known to occur along the Permian-aged Central European Basin's southern margin in Poland and Germany. Whereas production in the Mansfeld-Sangerhausen region of Central Germany ceased in 1990, the company KGHM Polska Miedz currently produces 0.5 Mt of Cu, 1000 t of Ag and significant quantities of precious metals and molybdenum annually in the Lubin region of SW Poland. Current mining operations in Poland are not only the single most important source of Cu in Europe but also the second most important source of Ag to global markets. Average copper grades in the Kupferschiefer deposits in Poland and Germany range between 1.5 and 2 wt.%, whereas average Ag grades are between 30 and 100 g/t.

The Spremberg-Graustein deposit is located ca. 100 km west of the Lubin mining region in the Lusatia region of Germany. The deposit was discovered in 1953 and intensively explored between 1953 and 1974 (Kopp et al., 2012). The Kupferschiefer-

40   type orebody at Spremberg-Graustein is located at a depth of ca. 900–1500 m and hosts at least 100 Mt of Cu-Ag ore with average grades of 1.5 wt.% Cu and 34 g/t of Ag (Kopp et al., 2012). Renewed exploration activity commenced in 2007. The Kupferschiefer Lausitz GmbH drilled a number of new exploration cores for resource confirmation purposes. These drill cores have been the subject of several mineralogical and petrographic studies (Minz, 2011; Lehmann, 2012; Stoll, 2014; Kehrer, 2016) providing valuable insight into the ore and gangue mineralogy of the Spremberg-Graustein deposit. However,

45   mineralogical characterisation, especially of the fine-grained gangue mineralogy, has proven difficult using traditional methods. Moreover, studies at the decimetre scale only provide sparse and discontinuous information, making it difficult to assess the spatial distribution of hydrothermal alteration and mineralisation.

In this study, hyperspectral drill core imaging (HSI) is used to characterise the effect of the hydrothermal alteration on the gangue mineralogy within and adjacent to stratabound Cu-Ag mineralisation in the Spremberg-Graustein deposit. We applied

50   visible to near-infrared (VNIR), short-wave infrared (SWIR), mid-wave infrared (MWIR) and long-wave infrared (LWIR) hyperspectral techniques to constrain the distribution of alteration mineral assemblages along three exploration drill cores. Infrared spectroscopy is based on the interactions of infrared light with molecules. The signals can be analysed by measuring absorptions, emissions and reflections (Burns, 1993; Harraden et al., 2013). Infrared spectrometers measure light at wavelengths covering the infrared domains reflected or radiating from the sample surface. In the SWIR and MWIR domains,

55   certain minerals have diagnostic absorption features (Thompson et al., 1999; GMEX, 2008; Laukamp et al., 2021). In the case of LWIR, it is possible to either measure reflected or emitted radiation. Mineral identification lies in the combination of characteristic spectral features and their distinction using subtle shifts in position, depth, or shape (Thompson et al., 1999; Jones et al., 2005; Harraden et al., 2013).

Hyperspectral mapping has been widely applied in mining and mineral exploration (e.g., Bedini, 2017). Extensive studies have

60   highlighted the relevance and the support HSI can provide to characteristic alteration mineral assemblages associated with hydrothermal ore deposits in magmatic (e.g., Herrmann et al., 2001; Jones et al., 2005; Zamuido, 2009; Riley et al., 2009; Ngcofe et al., 2013; Swayze et al., 2014; Kruse, 2015), orogenic (e.g., Bierwirth et al., 2002; Mateer, 2010; Laukamp et al., 2011; Arne et al., 2016; Wang et al., 2017) and in sedimentary environments (e.g., Taylor et al., 2005; Jakob et al., 2016). The benefits of this technology remain underexplored for hydrothermal ore deposits in sedimentary environments, such as

65   Kupferschiefer-type deposits. The present contribution builds on previous work on the hyperspectral characterization of similar deposits (e.g., Bedini, 2017; Lampinen et al., 2019) to (1) characterise the hyperspectral response of host rock and alteration mineral assemblages associated with Kupferschiefer-type mineralisation and (2) demonstrate the complementary nature of data collected over an extended hyperspectral range (VNIR, SWIR, MWIR and LWIR). The study places particular focus on three spectrally active mineral groups: the kaolinite, carbonate and iron-oxide groups. All three mineral groups have been

70   previously associated with hydrothermal alteration in the Kupferschiefer (Schmidt, 1987; Minz, 2011; Borg et al., 2012) and so have the potential to help map fluid pathways associated with stratabound Cu-Ag mineralisation.

2. Geological context

2.1. The Central European Permian basin

The Kupferschiefer is a thin but laterally persistent carbonaceous shale unit that is interpreted to mark rapid marine

75   transgression into the Central European Southern Permian Basin (CESB) at 257.3 ± 1.6 Ma. The CESB constitutes a network of aborted rift basins extending into the arid continental interior of the Supercontinent Pangea (McKie, 2017). It originated as an intracratonic foreland basin formed as a successor basin to the Variscan foredeep in the immediate aftermath of the Variscan Orogeny at the end of the Carboniferous Period (ca. 300 Ma, Coward, 1995; Borg et al., 2012).

The general stratigraphy of the basal infill in the southern part of the CESB (Figure 1), which is relevant for this study, can be
80 described as follows: The CESB infill overlies, with a marked erosional unconformity, basement lithologies that have been
variably deformed and metamorphosed during the Variscan Orogeny. The immediately overlying succession is of very variable
thickness and architecture; it comprises immature continental red beds and distinctly bimodal volcanic rocks of lower Permian
(Rotliegend) age. The top of the Rotliegend succession is typically represented by white to grey sandstones (Borg et al., 2012).
The deposition of the Kupferschiefer, a thin (usually less than a metre thick) but highly carbonaceous shale unit, occurred in
85 response to rapid marine transgression across the CESB and marks the contact between the terrestrial Rotliegend succession
and the conformably overlying marine Zechstein succession. From base to top, the Zechstein succession comprises the
Kupferschiefer *sensu stricto*, followed by several cycles of marine sedimentary rocks including dolostone/limestones,
anhydrite/gypsum and evaporites (McKie, 2017).
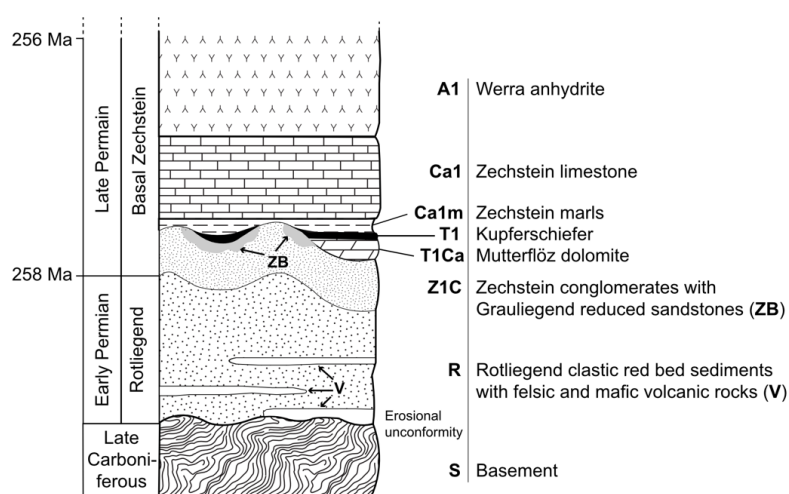
90 **Figure 1. Stratigraphic units in the southern part of the CESB (modified after Kopp et al., 2010).**

2.2. The Kupferschiefer: mineralisation and metallogenic model

The Kupferschiefer-type ore deposits in the CESB are classic examples of stratabound polyphase and polymetallic mineral
systems in sedimentary basins (Borg et al., 2012). Hydrothermal Cu-Ag mineralisation essentially centres around the
Kupferschiefer shale unit. The Kupferschiefer itself, the underlying sandstone, and the Zechstein limestone overlying the
95 Kupferschiefer *sensus stricto* may all be host to hydrothermal sulphide mineralisation, with a total thickness of the mineralised
interval ranging from less than 30 centimetres to more than 50 metres. The Kupferschiefer-type Cu-Ag ores are certainly of
polyphase origin (Borg et al., 2012); yet, the bulk of mineralisation is recognised to be mostly of dia- to epigenetic origin.
High-grade Cu-Ag- and subeconomic Pb-Zn-sulphide ores occur in increasing distance from a redox front that marks oxidative
alteration caused by metal-bearing hydrothermal basinal brines that likely derived their metal content from the Rotliegend
100 volcano-sedimentary basin infill below the Kupferschiefer (Kucha, 1990; Borg et al., 2012). The hematite-bearing oxidised
rocks, colloquially known as "Rote Fäule", mark the flow path of the metal-bearing brine towards the redox front as the site
of ore formation. The Kupferschiefer, with its high organic carbon content, acted as a geochemical trap and physical barrier
(Kucha, 1990; Borg et al., 2012; Speczik & Puttman, 1987). Metal sulphides precipitated from the brines wherever reducing
conditions prevailed beyond the extent of the redox front. Sulphide textures are exceptionally variable, ranging from
105 dissemination, impregnation, replacement and veinlet-hosted to semi-massive textured ores (Borg et al., 2012). The sulphide
ores show a distinct zonation, with local Au enrichment observed on the oxidized side of the redox front and Cu-Ag-rich ores
occurring immediately adjacent, but on the reducing side of the redox front. With increasing distance to the redox front, ores
become more Pb- and then more Zn-rich (Wodzicki and Piestrzyński, 1994; Schmidt, 1987; Borg et al., 2012).

The exact timing of hydrothermal fluid flow and Cu-Ag ore formation remains unclear. The diagenetic to epigenetic model presumes large-scale and multi-stage mass transfer through fluids systems active during different stages of the basin evolution, e.g., fluid convection in permeable sedimentary units during basin subsidence, progressive devolatilisation of the basin sequence and later fluid percolation during Cretaceous tectonic reactivation (Wodzicki & Piestrzyński, 1994; Schmidt-Mumm & Wolfgramm 2004; Borg et al. 2012).

2.3. The Spremberg-Graustein deposit

The Spremberg-Graustein deposit is situated near the south-eastern margin of the CESB in Lusatia, in the states of Brandenburg and Saxony, Germany (Fig. 2). The known deposit covers an area of ca. 14 km in length and 3 km in width and can be subdivided into two distinct portions, namely Spremberg and Graustein. These are separated by the so-called Türkendorf graben that has Cretaceous age (Kopp et al., 2006, 2008). The ore-bearing succession occurs 800 to 1500 m below present-day surface and dips gently toward the NE (Kopp et al., 2006, 2008). The well-mineralized zone is 2.4 m thick on average but locally reaches 8.2 m in thickness (Kopp et al., 2006). Cu-Ag resources are almost equally distributed between sandstones (ca. 31%), carbonaceous shale and marl (ca. 46%) and Zechstein carbonate rocks (ca. 23%); total metal content is estimated at 1.5 Mt of Cu with considerable quantities of Ag, Pb and Zn (Kopp et al., 2012).
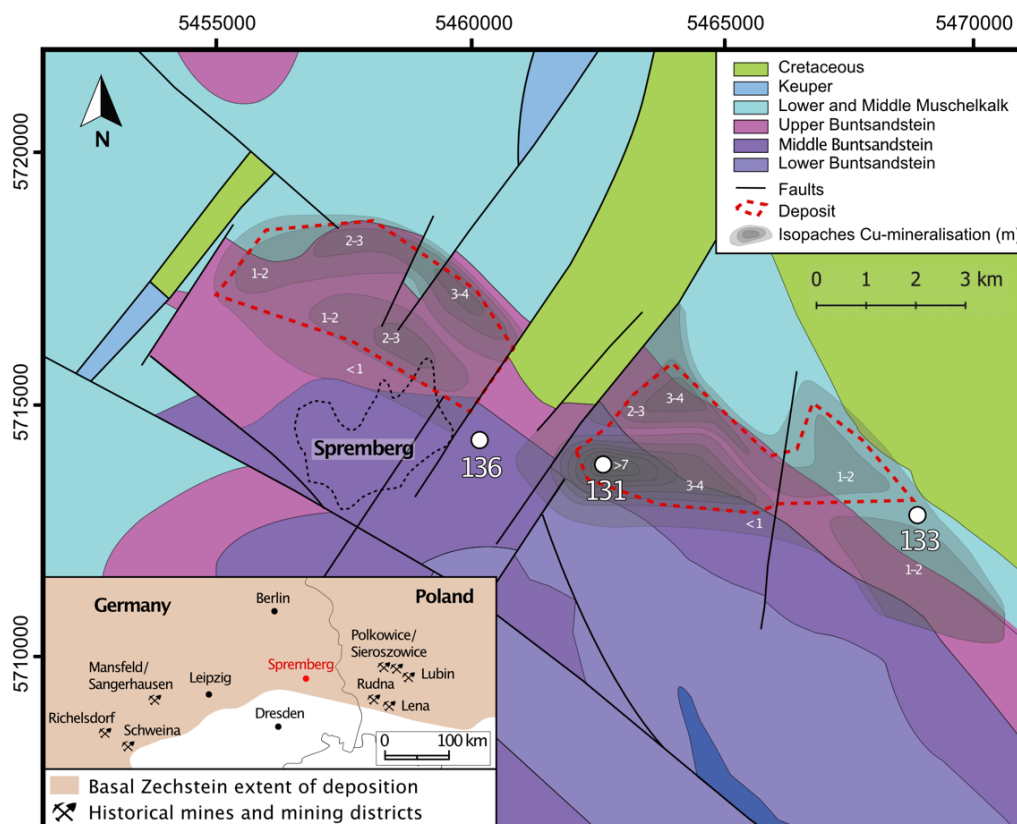
Figure 2. Geological map of the Spremberg-Graustein area showing the thickness of the economic Kupferschiefer-type mineralisation (after Kopp et al., 2006) and the location of the three drill holes that were subject of this study.

The mineralised succession is overlain by the Werra anhydrite succession that has a thickness of 200 m in total, followed by a 300 m thick Buntsandstein succession. The Muschelkalk and the Cretaceous successions are only preserved in the Cretaceous

Türkendorf graben structure, with the remainder removed by erosion. The Cretaceous-aged erosional unconformity is covered
130   by a blanket of Cenozoic sediments that is approximately 100 m thick (Kopp et al., 2006).

The Spremberg-Graustein deposit is located in the northern flank of the Mulkwitz structure, a horst developed during
Cretaceous SW-NE compression (Hartsch, 2015). The structure is bordered by NW–SE trending faults and subdivided by
numerous NE–SW trending faults (Kopp et al., 2012). The faults forming the Türkendorf Graben are synthetic NE–SW
downthrown faults (Franz et al., 1967) that were active during the lower Zechstein and from the Cretaceous to the Tertiary
135   (Hartsch, 2015).

This study focuses on mineralised intervals in diamond drill holes intersecting the Kupferschiefer near the town of Spremberg
(131, 133, 136, Fig. 2). Sandstone, shale (Kupferschiefer *sensu stricto*) and dolostone of the basal Zechstein succession are
intersected in all three drill cores. Drill core 131 is well mineralised, with grades above 0.8 % Cu in an 8 m long section and a
Cu grade of 8.7 wt.% in the Kupferschiefer *sensu stricto*. Drill core 133 exhibits economic copper grades only in the
140   Kupferschiefer *sensu stricto*, reaching a maximum of 3.9 wt.% half a metre above the sandstone-shale contact. Drill core 136
is less well mineralised. It contains two spatially distinct sections of mineralisation with grades of 0.33 wt.% and 1 wt.% Cu,
respectively: one at the contact between shales and sandstone and another 4 m above in limestones (Fig. 3). Cu mineralisation
comprises of Cu- and Cu-Fe-sulphides, including chalcocite (Cu_2S), digenite ($Cu1.75S5$), covellite (CuS), bornite (Cu_5FeS_4),
and chalcopyrite ($CuFeS_2$) (Kopp et al., 2006; Spieth, 2019).

145
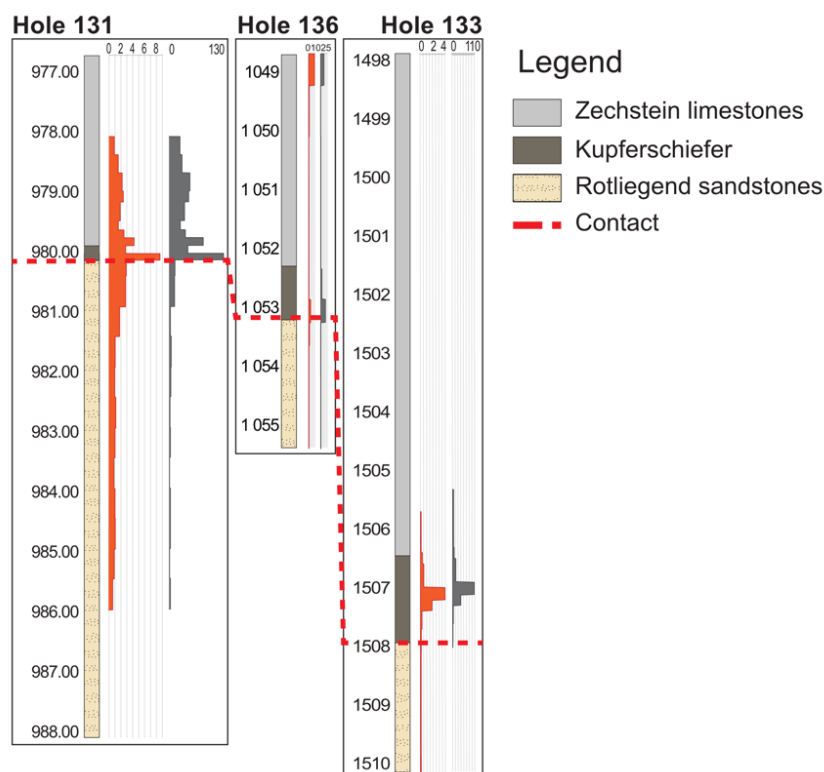
Figure 3. Lithology, copper (red in wt.%) and silver (grey in g/t) grades in the drill cores available for this study.

2. Methods

2.1. Data acquisition

150 Hyperspectral data was acquired for each of the three drill cores using a SisuROCK drill core scanner (Fig. 4) equipped with SPECIM AisaFENIX, FX50 and AisaOWL hyperspectral push-broom sensors (Spectral Imaging Ltd., Oulu, Finland; Table 1). The scanner is equipped with internal lighting and a moving tray that moves under the scan line of each sensor. Dark current corrections are used to remove hot pixels and other fixed-pattern noise. We used a grey panel (Spectralon R50) as reference instead of conventional white panels (e.g., Spectralon R90) panel as longer integration times were required, to improve the

155 signal-to-noise ratio of the overall dark shales and carbonates.

Figure 4. (A) Specim SisuROCK hyperspectral drill core scanner with (B) mounted sensors in the visible to near-infrared and short-wave infrared (VNIR-SWIR), mid-wave infrared (MWIR), and long-wave infrared (LWIR) range.

Table 1. Acquisition parameters of the SisuROCK drill core scanner.

	VNIR	SWIR	MWIR	LWIR
SPECIM camera	AisaFENIX	AisaFENIX	FX50	AisaOWL
Wavelength range	380–970 nm	970–2500 nm	2700–5300 nm	7700–12300 nm
Bands (binning)	175 (4)	275 (1)	154 (1)	96 (1)
Spatial resolution	1.50 mm/px	1.50 mm/px	1.06 mm/px	1.60 mm/px
Calibration	Grey panel		Thermic calibration	

160 ### 2.2. Image processing

The acquired hyperspectral data was preprocessed using *hylite* (Thiele et al., 2021) to (1) convert from radiance to reflectance, (2) apply geometric correction to remove lens distortions, and (3) co-register the data from different sensors. After coregistration, background pixels were manually masked from each tray and the images mosaicked (per sensor and drill hole) for subsequent analyses.

165 Hyperspectral data can be used to derive quantitative mineral maps where appropriate training data is available (Tusa et al., 2020; De La Rosa et al., 2021) but the preparation of training samples usually takes days or weeks. This study focuses on spectral tools that can be rapidly applied for qualitative mapping and interpretation. In this study, we identify and map the position or depth of specific absorption or emission features, which are known to correspond to relevant minerals or elements. Key minerals that can be spectrally identified in the Kupferschiefer are outlined in Tables 2 and 3. We used band ratios and

170 minimum wavelength mapping, implemented in *hylite* (Thiele et al., 2021) to identify minerals characteristic of a lithological unit or the products of hydrothermal alteration. For simplicity reasons, we refer to these diagnostic minerals as proxies. Band ratios are a simple and robust technique for identifying spectral features. In its simplest form, the reflectance measured at the wavelength corresponding to the shoulder of an absorption feature is divided by the reflectance measured at its minimum, giving values equal to 1 if no absorption is present and larger values as absorption depth increases. For example, with iron

175 indices, such as 600/570 nm for Fe^{3+} and (920 nm + 1650 nm) / (1230 nm +1035 nm) for Fe^{2+} (Cudahy et al., 2008), we can

quantify the depth of two broad but characteristic absorption features in the VNIR and SWIR range, present respectively in the 500–750 nm range and the 750–1400 nm range (GMEX 2008, Laukamp et al., 2021). The band ratios we applied to characterise the Kupferschiefer cores are listed in Table 2.

180 **Table 2. Spectral indices for relevant proxies in the Kupferschiefer and its host rock succession at the Spremberg-Graustein deposit.**

Feature	Ratio (in nm)	Mask	Interpretation	Reference
Fe^{3+} index	600/570	R > 1.1 to overcome surficial oxidation (storage)	Depth of the Fe^{3+} absorption from e.g., hematite, goethite	GMEX (2008)
Fe^{2+} index	(920+1650) / (1230+1035)		Broad absorption centred at ~1000 nm can be influenced by ferrous iron in silicates and carbonates.	Cudahy et al. (2008)
Kaolinite index (KI)	2209/2170	(2138+2190) / (2156+2179) >1.005	KI close to 1 suggests pure kaolinite, lower values are associated with poorly crystalline kaolinite or illite-kaolinite mixtures	Laukamp et al. (2011)
Anhydrite index (AnI)	8661/9156	R > 1.1	Second slope of the anhydrite peak feature	Kokaly et al. (2017)

Minimum wavelength (MWL) mapping fits spectral absorption features using one or more simple mathematical functions, in our case asymmetric Gaussian functions (Thiele et al., 2021), to resolve a measured (and hull-corrected) spectrum into specific absorption positions and depths (Van der Meer et al., 2004; Van Ruitenbeek et al., 2014). For example, three Gaussian

185 functions can be fitted to hull-corrected reflectance spectra in the range 2100–2400 nm. The relative depth and position of these functions are used to constrain the likely mineral mixtures present. As the combined depth and position (wavelength) of these features is informative, minimum wavelength maps are commonly visualised using hue to represent feature position and brightness to represent feature depth. Minerals with diagnostic absorption features (e.g., gypsum, which has a diagnostic absorption at 1750 nm) can be qualitatively identified using feature depth alone. Minerals with overlapping spectral features

190 (e.g., calcite and dolomite) can only be discriminated by combining absorption depth and position information. The main spectral ranges that were mapped using the MWL technique, and our interpretation of the resulting features, are listed in Table 3.

Table 3. Spectral ranges used to extract the position and depth of specific absorption and emission features using minimum wavelength mapping techniques.

Spectral range (nm)	Expected features	Interpretation	Reference
1740–1770 (1 minimum)	~1750 nm	Diagnostic absorption feature associated with gypsum.	Laukamp et al. (2021)
1800–2400 (fit with 4 minima)	~1900 nm	Absorption feature associated with water molecules in e.g., clay minerals	GMEX (2008); Kokaly et al. (2017); Laukamp et al. (2021)
	~2160 nm	Doublet associated with kaolinite	
	~2200 nm	AlOH absorption associated with clay or mica minerals.	
	~2330 nm	Absorption associated with carbonate minerals and AlOH or MgOH bearing silicates (e.g. clays/micas). Position can be used to distinguish dolomite, calcite and clay/micas.	
3500–3650 (1 maximum)	~ 3700 nm	Feature similar to a peak, but shaped by the two carbonate absorption features present on its side at ~ 3800 and ~ 3900 nm	Kokaly et al. (2017); Laukamp et al. (2021)
3700–4100 (1 minimum)	~ 3900 nm	Second absorption feature of the carbonates doublet between 3780 and 4080 nm	Laukamp et al. (2021)

4350–4600 (1 minimum)	~ 4470 nm	Quartz absorption feature	Laukamp et al. (2021)
7731–9427 (1 maximum)	~ 8200 nm	Quartz primary reststrahlen band peak feature	Kokaly et al. (2017); Laukamp et al. (2021)
10800–11600 (1 maximum)	~ 11300 nm	Carbonate peak feature	Green and Schodlok (2016)

2.3 Micro-XRF validation

Micro-X-ray fluorescence (XRF) is a spatially-resolved, non-destructive technique for the elemental analysis of geological samples (Berdan et al., 2019). It benefits from the combination of element-specific X-ray fluorescence detection and rasterized data acquisition. The generated elemental maps can be used as training data to derive mineral abundance from HSI (Barker et al., 2020). In this study, we use XRF elemental maps for the qualitative and quantitative geochemical validation of hyperspectral mineral maps. Data acquisition and processing were performed using a BRUKER M4 Tornado XRF spectrometer at the Helmholtz Institute Freiberg for Resource Technology. An excitation beam of 20 m was generated by applying a high voltage (50 kV) to a Rhodium anode and focussed on the sample surfaces by polycapillary lenses. XRF signals emitted by the samples were collected for 70 ms by two detectors (count rate: 275 x 10^3 counts per second each) at a spatial resolution of 300 μm per pixel, obtaining distribution maps for elements heavier than Na. We obtained quantitative estimates for element concentrations using the BRUKER M4 Qmap tool, which relies on Fundamental Parameters (FP) models for standardless quantification of elements and compounds present in XRF elemental maps. FP models are particularly useful when certain elements cannot be directly measured due to limitations inherent to the equipment (e.g., elements lighter than Na) and are dependent on the sample's elemental composition, instrument-specific information, mathematical constants and known stoichiometric ratios (BRUKER, 2020). For this study, we did assume that all elements considered (Al, Ca, Cu, Fe, K, Mg, Mn, O, Pb, S, Si, and Zn) are present as oxides, and hence generate oxide abundance maps. This is despite the fact that it is safe to assume that Cu, Pb and Zn are all present as sulphides - and that sulphur may be present as sulphide or as sulphate.

3. Results

The spectral proxies described in the previous section (Section 2.2) characterise the distribution of the main rock-forming and alteration minerals in the three studied drill cores. These have been assembled and plotted on a graphic log (Appendix 1), and an averaged 10-cm resolution downhole log (Appendix 2) to allow easy comparison and interpretation.

Previous studies have revealed that the mineralised Kupferschiefer *sensu stricto* in Lusatia and SE Poland comprises of a very fine-grained mixture of clay-sized (< 2 μm) sheet silicates (illite, kaolinite, chlorite, dickite), carbonate minerals (ankerite, minor calcite, prominent dolomite), organic matter and sulphides (chalcocite, bornite, covellite, digenite, chalcopyrite, djurleite) (Rahfeld et al., 2018; Kehrer, 2016). Owing to the abundance of organic matter the Kupferschiefer *sensu stricto* is of dark grey to almost black colour; its response to HSI is thus quite flat with very low reflectance and unspecific. The same limitation does not apply to the sandstone and the Zechstein carbonate rock. Key observations on these two lithologies are summarised below.

3.1. Quartz

Quartz was mapped using two features: the widely applied emission peak at ~8200 nm in the LWIR range, and a less well-known feature at F4500 nm in the MWIR (Fig. 5). The latter, present more precisely at ~4470 nm, hasn't been extensively studied so far but it is likely related to the presence of quartz (Laukamp et al., 2021). This is in good agreement with the results in this study as this feature is detected mostly in the quartz-rich sandstones. This absorption feature is locally also present in the dolostones and may allow the detection of minor quartz in this carbonate rock. Yet, the signal seems too weak and sparse to be reliable.
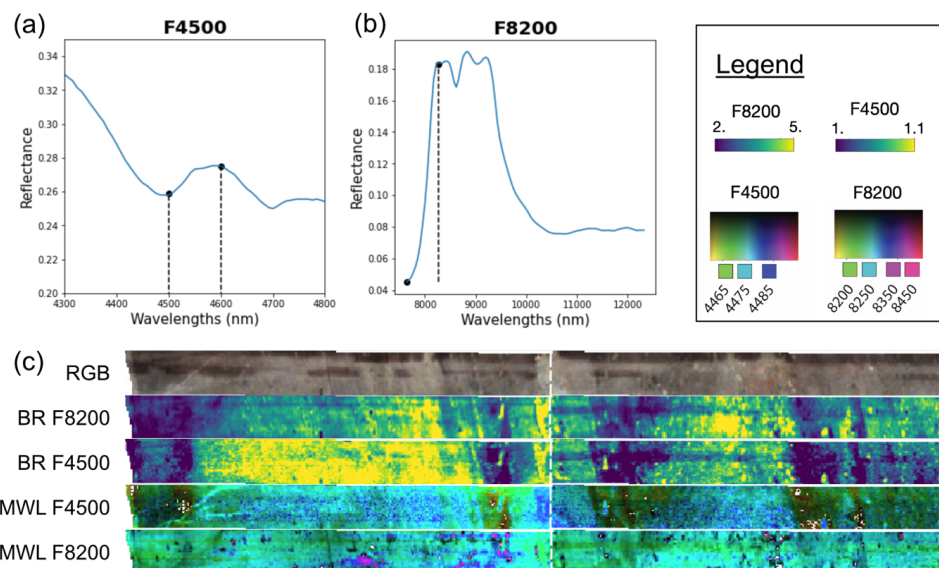
Figure 5. Distribution of the quartz-related spectral features in the Kupferschiefer cores. (A) Band ratio for F4500; (B) band ratio for F8200; (C) RGB, F8200, F4500 maps for drill hole 136 (depth from right to left = 1053.5–1055.5 m, sandstones)

Both band ratio and MWL techniques were used to quantify these two features. The quartz emission peak occurs in all the sandstones of the three studied boreholes. However, this feature is not present in the Zechstein limestones because quartz abundance is minor and mostly restricted to stylolites (Lehmann, 2012; Stoll, 2014). The band ratio approach appears to provide more reliable results, with the MWL method showing strong sensitivity to overlapping features. The band ratio for 8200 nm on the first slope of the primary reststrahlen band shows a good correlation with the band ratio implemented on the second slope of the 4500 nm absorption (Fig. 5). In the sandstones of hole 136, the F8200 emission peak is locally shifted toward higher wavelengths, having a maximum at 8350 nm or 8450 nm. However, in the two other boreholes, the F8200 position is always between 8200 and 8250 nm. This difference may be due to the contrasting crystallographic orientation of the quartz in the respective drill cores (Tappert et al., 2013). Alternatively, based on the correlation of F8200 with the anhydrite map (Sect. 3.3), the feature shift in hole 136 could be the result of interference with the 8350 nm sulphate emission peak (Kokaly et al., 2017) in anhydrite-rich areas. The F4500 feature is a reliable quartz indicator in sandstones, but more cryptic in the carbonate rocks. In the sandstones, this absorption mainly occurs at 4475–4485 nm but is shifted to 4465 nm where carbonates give a significant spectral response suggesting it interferes with absorption features related to carbonates. This may be due to the overlapping with dolomite absorption at ~4440 nm (Kokaly et al., 2017). Quartz features in the mid-wave domain (i.e., F4500) and in the long-wave domain (i.e., F8200*) are present all along the sandstone sections of the three holes, suggesting that both are persistent even in mineral mixture cases. However, if dolomite is present (with an MWIR absorption at 4430 nm; Kokaly et al., 2017), the position of the F4500 quartz feature is shifted toward shorter wavelengths (cf. Appendix 1). In a ten-centimetre-long region at the contact of 131 and 136, the F4500 quartz feature is less prominent due to lower reflectance, possibly due to high sulphide content.

3.2. Carbonate minerals

The SWIR, MWIR and LWIR ranges all contain spectral features that can be used to characterise carbonate mineralogy. The most well-established of these is the 2320 (dolomite) to 2345 nm (calcite) absorption feature in the SWIR range (Gaffey, 1986; Laukamp et al., 2021). This SWIR-based index shows that the basal Zechstein carbonate rocks are dominantly calcitic in drill cores 136 and 133, and dolomitic in drill core 131 (Appendix 1). It is interesting to note (but possibly coincidental) that hole

131 is also the best mineralised of the three holes. This carbonate feature shows that carbonate forms the dominant cement in some parts of the sandstones, as has been previously described in these rocks and elsewhere (Wodzicki and Piestrzynski, 1994; Minz, 2011) and that this cement appears to be calcitic in hole 131 and 133 and more dolomitic in 136. However, note that the

260 interpretation of carbonate and clay cement mixtures is complicated by the presence of an overlapping absorption feature of many clay minerals with the main spectral feature of carbonate at ~2340–2350 nm.

The carbonate absorption features in the MWIR and LWIR range are less well studied, though have previously been identified as complementary to those in the SWIR (Laukamp et al., 2021). To explore this potential, 10-cm averaged depth and position for each of the four carbonate absorptions were computed and compared (Fig. 6).
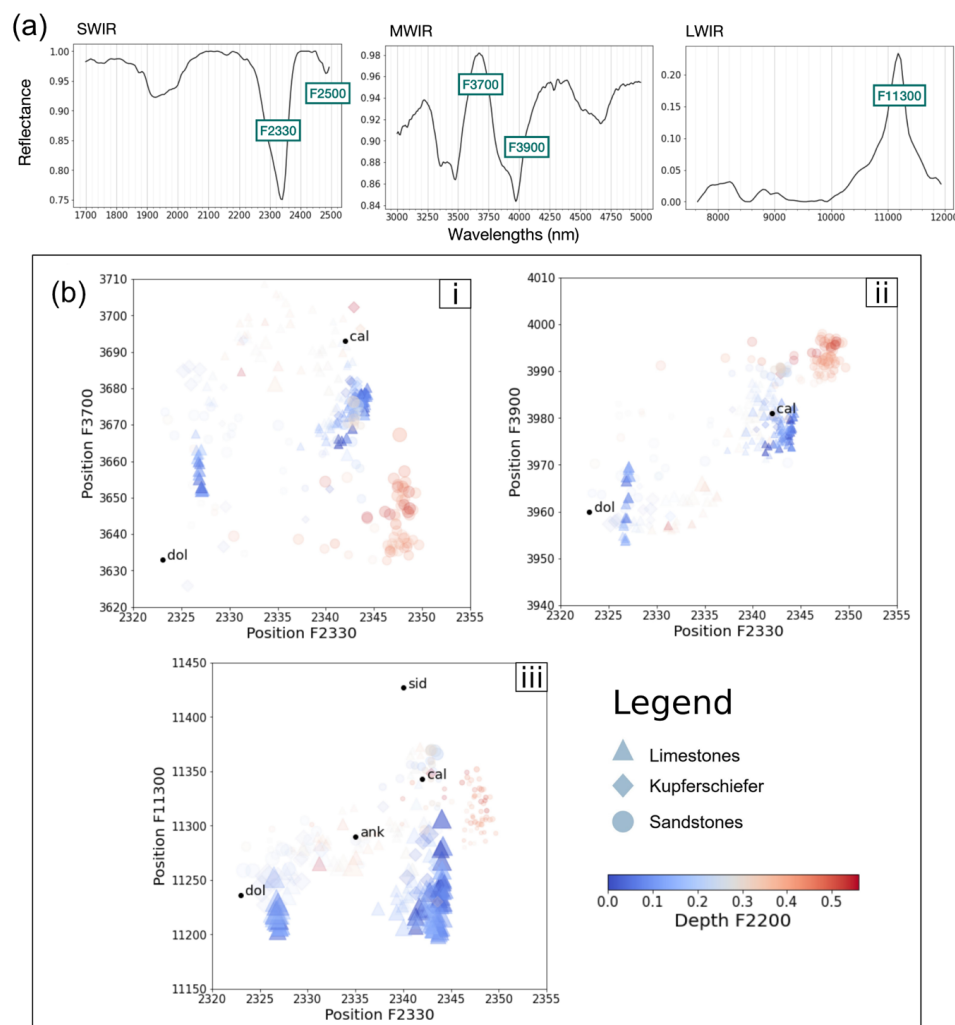
265

Figure 6. Example spectra (A) showing the dominant carbonate absorption positions in the SWIR-MWIR-LWIR spectral range. The 10-cm averaged position of these features (i. F3700; ii. F3900; iii. F11300) are plotted in (B) using the F2330 feature as a reference. Size is proportional to the depth of the feature on the y-axis and transparency to the depth of the F2330 feature. Colour indicates the depth of the F2200 feature and serves as a proxy for clay mineral abundance. Black points (cal=calcite; dol=dolomite; sid=siderite; ank=ankerite) show reference positions from the USGS spectral library (Kokaly et al., 2017) and Green and Schodlok (2016) for F11300.

270

The precise position of these varies, but for simplicity, they are referred to here as F2330, F3700, F3900 and F11300. The SWIR-based index clusters the carbonate-bearing lithologies into three main groups: dolomitic (2325 nm), calcitic (2340 nm)

275 and clay-rich (2350 nm), the latter with deep a AlOH feature. It becomes increasingly difficult to distinguish these clusters using higher wavelength features. However, this suggests that the combination of features could be used to identify distinct subpopulations within each of these three clusters and hence provide complementary information. In the MWIR range, the dolomite spectra show significant variation, ranging from 3650 to 3680 nm for the F3700 feature and 3950 to 3970 nm for the F3900 feature. The cause of this variation is unclear but could reflect a sensitivity to, e.g., grain size and crystallinity, and

280 potentially different dolomite generations that have been documented in the mineralised sandstones (Minz, 2011) and Zechstein carbonate rocks (Lehmann, 2012). The LWIR spectra show even more variation, especially in the calcitic group, which spans 11200 to 11375 nm, to the point where dolomite and calcite are no longer distinguishable without other information. It has been well established that long-wave spectra can be sensitive to confounding factors such as grain size and orientation (Zaini et al., 2012).

285 Significant variations in the iron content of these carbonates, as indicated by the iron Fe^{2+} index in this study, can also contribute to the variation in the MWIR and LWIR ranges (Fig. 7). The position of the MWIR carbonate feature F3900 is shifted toward higher wavelength when the Fe^{2+} index indicates high ferrous iron abundance (Fig. 7).
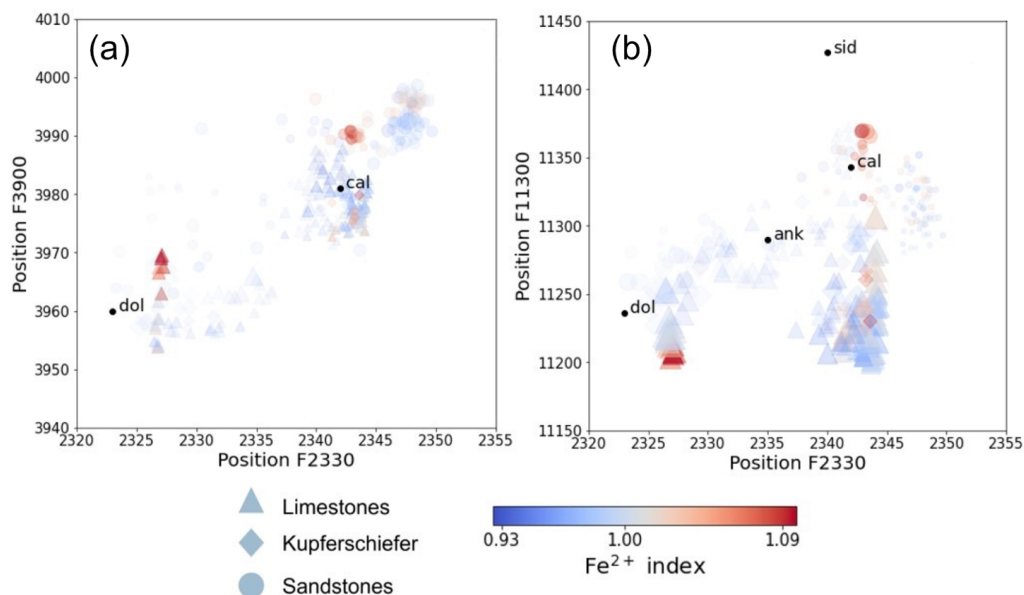
Figure 7. The 10-cm averaged position of carbonate-related spectral absorption features (A) F3900 and (B) F11300 plotted using the
290 **F2330 feature as a reference. Size is proportional to the depth of the feature in the y-axis and transparency to the depth of the F2330 feature. Colour indicates the value of the ferrous iron feature (Cudahy et al., 2008) and appears to account for some of the variation observed in the MWIR and LWIR.**

Interestingly, the position of the carbonate features (especially in the MWIR and LWIR range) appears to change in the vicinity
295 of well-developed stylolites. These changes are particularly pronounced in hole 136. The shift of the carbonate feature in the LWIR (at ~11300 nm) reveals zoned halos around stylolite joints where the feature is shifted toward higher wavelengths. The same trend is observed for the carbonate feature in the MWIR domain at ~3700 nm. Generally, these shifts occur where limestones are mineralized. µ-XRF maps of two samples were produced for a better understanding of these features.

µ-XRF results (Fig. 8) show that the iron and silicon content are spatially correlated.
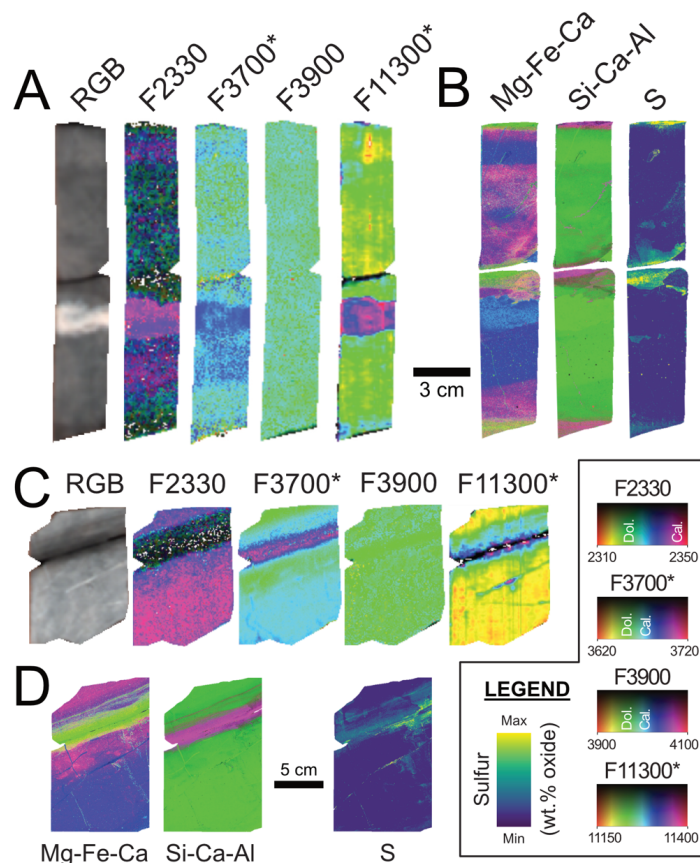
Figure 8. Comparison of hyperspectral imaging (HSI) data and spatially-resolved chemical (µXRF) data for validation. (A) HSI data for sample 1 from drill core 136, 1048.7–1048.85 m depth, and (B) corresponding µXRF data displayed as false-colour RGB images. (C) HSI data for sample 2 from drill core 136, 1049.4–1049.5 m depth, and (D) corresponding µXRF data.

Where iron and silicon are detected by µ-XRF in sample 2, the position of both features F3700 and F11300 is shifted toward higher wavelengths. However, in sample 1 this trend is poorly pronounced for F11300 and even not observed for F3700. It seems that the F3700 position stands for calcite and dolomite, by comparison with F2330 and µ-XRF, but it may be influenced by silicate occurrence at stylolite joints, as it is suggested by elevated Si contents in sample 2. Si in stylolite joints ioccurs as quartz, micas, and feldspar (Lehmann, 2012). Those observations indicate that the F3700 position is mainly influenced by carbonate composition between dolomite and calcite, but it is shifted toward higher wavelengths when carbonate is present together with silicates. We observe a larger variation of F11300 along veins, stylolite joints and concretions, with no clear correlation with a given element, indicating that this feature might be texture-related (e.g., grain size and orientation) in this context.

Quantitative X-ray powder diffraction (QXRD) results published by Kehrer (2016) and shown in Appendix 1 corroborate the hyperspectral observations by showing that dolomite is dominant in hole 131 (65.7 wt.% dolomite vs 1.75 wt.% calcite). In contrast, calcite dominates samples from the top of hole 136, with dolomite becoming significant (51.5 wt.%) towards the contact with the Kupferschiefer. No QXRD analysis was carried out on drill core 133.

Kucha (1990) describes the mineralised, top part of the sandstones immediately below the Kupferschiefer in the Polish deposits as cemented by sulphides and carbonates. Carbonate cement is identified in holes 131 and 136, where F2330, F3900 and F11300* are present in the same regions close to the contact with shales. In the sandstones section of 133, F2330 overlaps

with the illite absorption doublet, and hence cannot unequivocally be attributed to carbonates. However, the two carbonate features in the MWIR, F3700* and F3900, are present all along the three sandstone sections. For F3700*, we locally observe a shift towards shorter wavelengths that may indicate the presence of dolomite and calcite cement (Fig. 6). In 131 and 136 sandstones, F3700* shifts to higher wavelengths in regions where F1750 is present. This suggests that this carbonate absorption

325   position may be affected by a mixture with sulphate minerals. This effect requires further investigation. Furthermore, the F3700* peak' feature is shaped by the two carbonate absorptions. The shift of F3900 exhibits only two different positions in the sandstones (and also in the two other lithologies) and, in 131, QXRD and mineral liberation analysis (MLA) confirms (Kehrer, 2016) that the position 3960 and 3985 nm are for dolomitic and calcitic cement respectively.

3.3. Sulphate minerals

330   Spectral proxies for gypsum (1750 nm absorption feature) and anhydrite (8661 nm emission peak) show isolated pockets of nodule-like sulphate minerals within the footwall sandstones and overlying carbonate rocks. While these two spectral indices allow gypsum to be distinguished from anhydrite, we suspect that surficial anhydrite has been converted to gypsum during core storage, so we consider them to represent equivalent sulphate minerals. That said, the 1750 nm (gypsum) absorption feature appears more widely distributed (and is often relatively disseminated) compared to the distinct anhydrite nodules

335   mapped by the 8661 nm emission peak in the Zechstein limestone units (Fig. 9B). Anhydrite detection in sandstones is not possible because of an overlap with the quartz feature. It is possible that the band ratio highlights the presence of diagenetic sulphate nodules. Kucha (2003) described these nodules as anhydrite ± gypsum ± calcite nests.

Gypsum absorption is very short (0.02 to 0.05 reflectance contrast) but maps show patterns such as layers or veins ensuring this feature has trustworthy geological significance. Though, gypsum occurs in the studied material with a low concentration

340   of about less than 1 wt.% in the dolostones and the Kupferschiefer and of about 5 wt.% in the sandstones according to XRD (Kehrer, 2016). This indicates gypsum has a strong spectral answer and it can be detected in the mineral mixture even with low concentrations.

Within the sandstones, sulphates occur as cement (Kucha, 1990) and the F1750 absorption mapping potentially allows the detection of such sulphate minerals. The F1750 map shows small nodules (close to the mm resolution of the scanner)

345   concentrated along distinct bedding horizons within cross-bedded portions of hole 131 (Fig. 9). The correlation between the 1750 nm absorption feature and gypsum in hole 131 has been validated by comparison with QXRD results from Kehrer et al. (2016) (Fig. 9C and D). Sulphates appear comparatively disseminated within the sandstones of holes 136 and 133, but are still present at detectable levels. The spatial extent of F1750 in sandstones of drill core 136 inversely correlates with the occurrence of carbonate spectral features, suggesting that HSI possibly allows the distinction of sulphate-rich cement to carbonate-rich

350   cement.
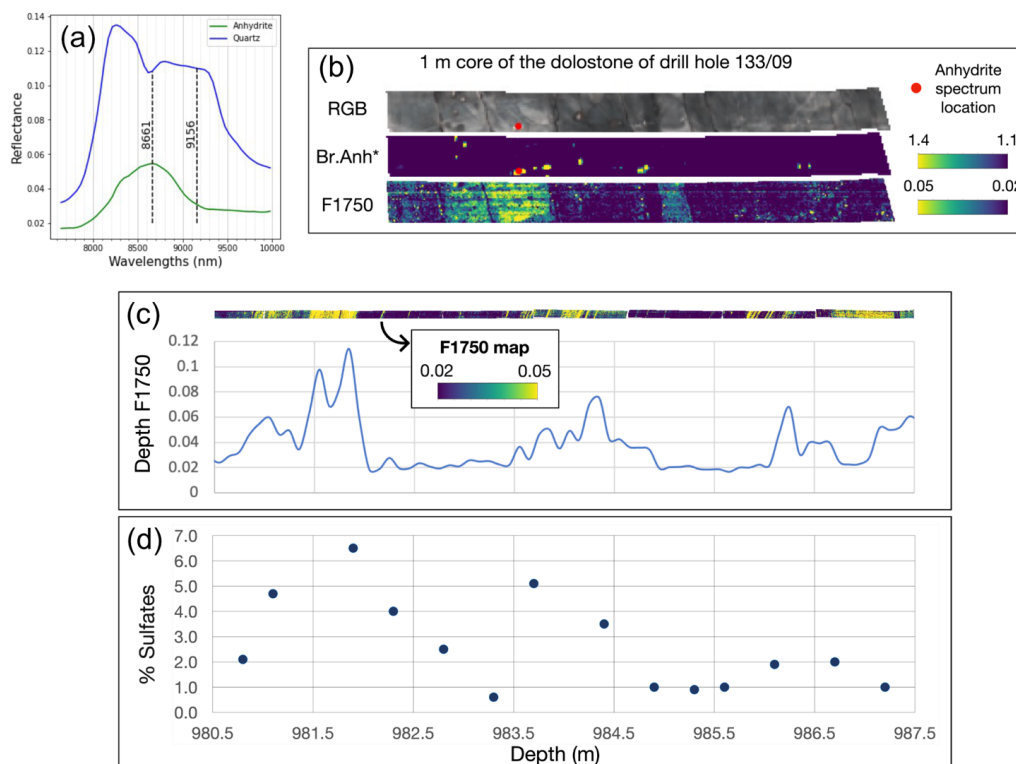
Figure 9. (A) Anhydrite spectrum at a pixel in an anhydrite nodule within the Zechstein limestone, and bands involved in the band ratio Anhydrite index (black dashed lines), in a section of 133 at a depth of ~1498 m (B). (C) F1750 map and plot of the averaged depth of F1750 every 10 cm in 131 sandstones and (D) QXRD wt.% sulphates results (Kehrer, 2016).

355

3.4 Micas/clays

The general abundance of mica and clay minerals are mapped by the depth of the 2200 nm absorption associated with the Al-OH complex (Laukamp et al., 2021; GMEX, 2008). Unsurprisingly, these show that mica/clay minerals are far more abundant in the sandstone than in the limestones. Locally, bands of darker-coloured limestone in drill cores 133 and 136 are found to

360 contain detectable amounts of clay. The presence of clay/mica minerals in these bands (Fig. 10) is corroborated by QXRD results of Kehrer (2016). Similarly, local enrichment of mica in the dolostone is found directly above the mineralised zone in drill core 131 has been identified by QXRD analysis (Kehrer 2016); this is confirmed by the F2200 absorption feature (Fig. 10A).
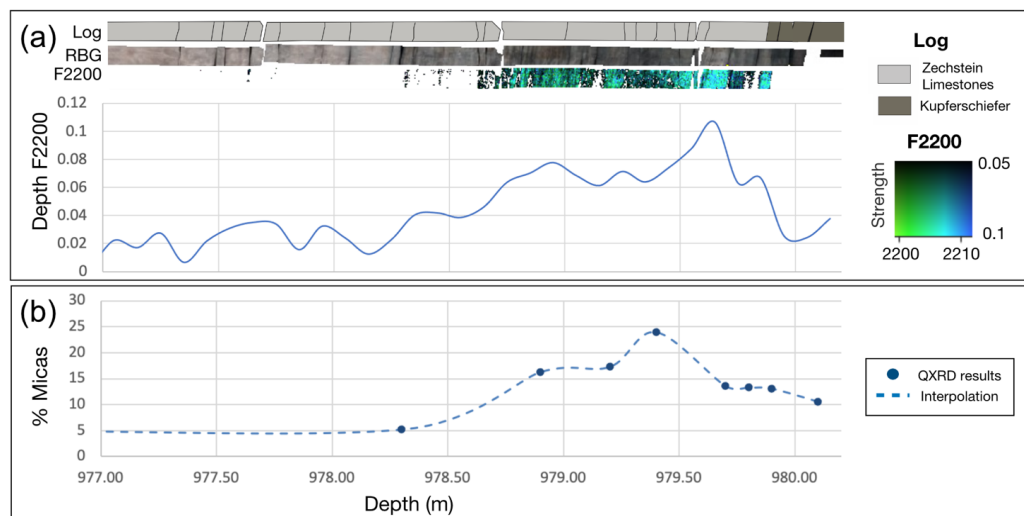
Figure 10. Distribution of the mica/clay-related absorption feature in the Kupferschiefer cores. (A) Log, RGB and F2200 map in the limestone and Kupferschiefer of drill core 131 and (B) results of QXRD for micas (from Kehrer, 2016).

365

In the sandstones, the kaolinite spectral index indicates the presence of relatively crystalline (and hence likely hydrothermal) kaolinite in distinct zones close to the base of the Kupferschiefer. This is especially pronounced in hole 131 (Fig. 11) and correlates with petrographic measurements made by Minz (2011). The kaolinite index suggests a similar trend in hole 136,

370 crosscut by distinct kaolinite-rich veinlets or fracture zones which provides further evidence that the origin of high-crystallinity kaolinite postdates diagenetic lithification. Kaolinite is almost absent in hole 133, where mineralisation is confined to a copper zone within the Kupferschiefer horizon and a lead-rich zone in the overlying carbonates.

The barren sandstones in drill core 133 are spectrally different from the two other drill cores because they exhibit phengite-type spectra in the SWIR domain. Well-mineralised sandstones of the two other drill cores (131 and 136) display spectral

375 characteristics for illite and kaolinite mixtures. In this drill hole, the sandstone occurs at an interval about 500 m deeper compared to the other two. Therefore, conversion of kaolinite to illite may have occurred during deep burial diagenesis associated with elevated temperatures, compaction and dewatering of shales (Hancock & Taylor, 1978; Mantovani et al., 2010).
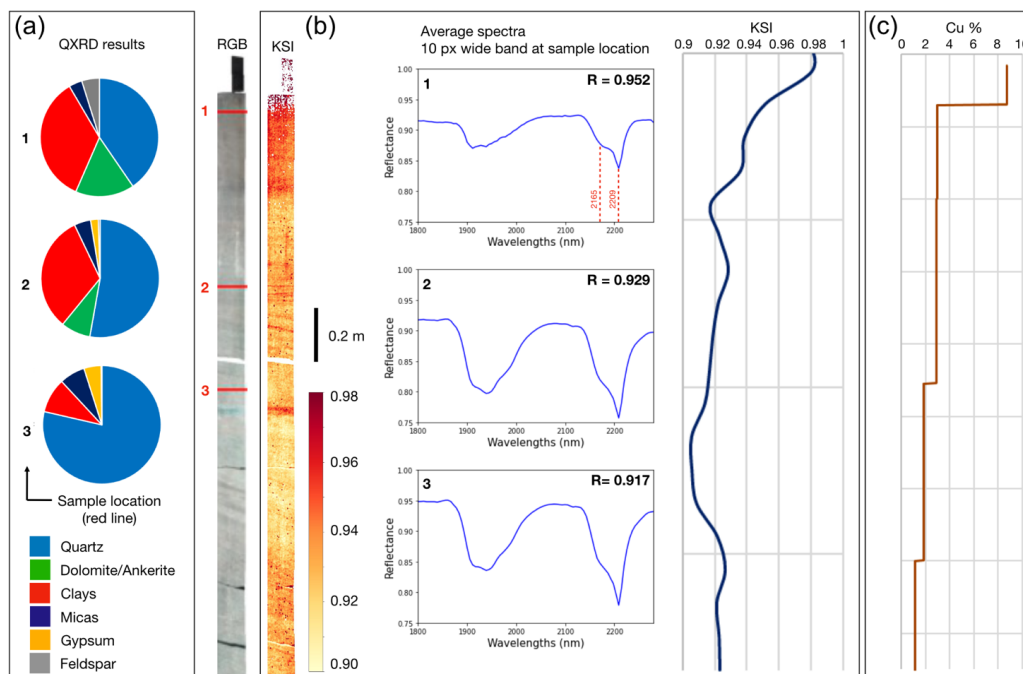
Figure 11. (A) QXRD results (Kehrer, 2016) for 3 samples at various depths in drill core 131 (1, 2 and 3); (B) KI map sandstones and organic-rich shales; average spectra in a 10 pixels wide band (≈ 1 cm) at QXRD samples location; KI average along the core and (C) copper grade.

The dominance of kaolinite vs illite-kaolinite mixtures can be assessed using the KI. Based on a careful petrographic study Minz (2011) suggested kaolinite in the mineralised sandstones of the Spremberg-Graustein deposit to be the product of kaolinitisation of feldspar. This reaction yielded well crystalline kaolinite filling intergranular pores spaces in paragenesis with Cu sulphides, carbonates and euhedral quartz. Minz (2011), therefore, regarded the kaolinite to be cogenetic with Cu-Ag mineralisation (Minz, 2011; Schmidt, 1987). HSI imaging reveals that KI increases towards the mineralized contacts of sandstone and Kupferschiefer *sensu stricto* in drill cores 131 and 136. Previous MLA and QXRD results (Kehrer, 2016) also report a relative increase of clay minerals in sandstones towards the contact with the Kupferschiefer *sensu stricto* in both drill cores. However, the relationship between KI and clay/micas abundance is not linear. The KI appears to reflect clay occurrence, and to a lesser extent, it may be indicative of the relative amount of clay vs mica. Our results also show that the KI may be influenced by kaolinite crystallinity (GMEX, 2008).

3.5 Iron

Both the Fe^{3+} as well as the Fe^{2+} index may be indicative of the effects of hydrothermal alteration in the Kupferschiefer mineral system. The Fe^{3+} index (600/570 nm) identifies the transition from bleached and/or sulphide mineralised sandstones into sandstones that are red discoloured by hematite near the bottom of all three drill cores (see core 131 in Fig. 12 as an example). This is consistent with previous core logging results as the presence of hematite is easily identified by its distinct reddish colour. In drill core 136, the presence of hematite is rather patchy than pervasive. Interestingly, in drill core 131 the transition from hematite-bearing to hematite-absent sandstones is gradational with a transition over ~2 m, whereas more patchy hematite alteration is developed in drill cores 136 and 133, showing remarkably sharp top and bottom contacts. It is important to note here that the mere presence of hematite in the sandstones is not regarded here as unequivocal evidence of hydrothermal alteration. In fact, the observations made during this study on only three drill cores make it impossible to distinguish clearly

between hematite that is a product of sedimentation and diagenesis of the Rotliegend red bed sediment succession from
405   hematite that may have formed as a product of hydrothermal alteration (e.g., the Rote Fäule).
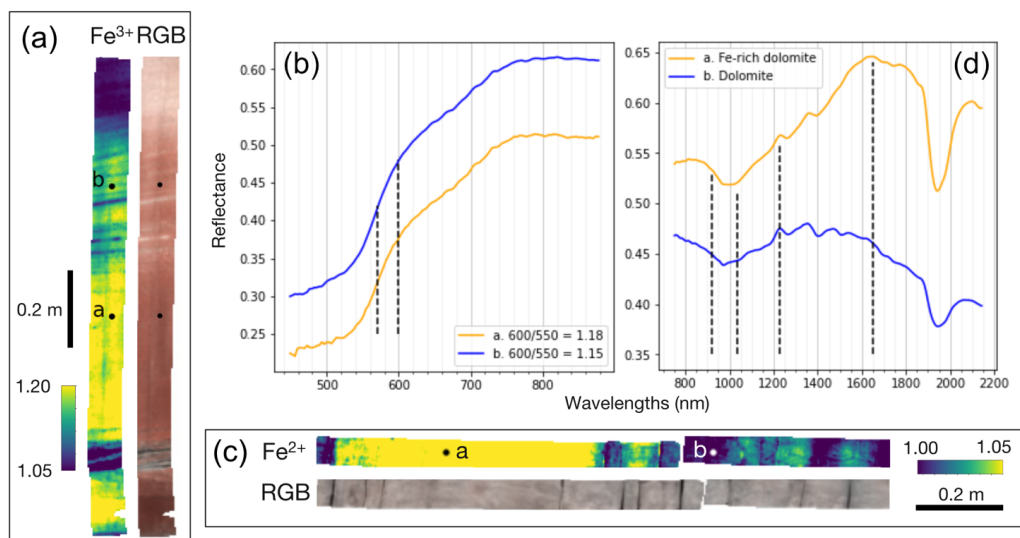
Figure 12. (B) average (5x5 pixels) spectrum at location a and b in (A), of hematite-bearing sandstones in drill core 131 (987.2–988.2 m depth). **(D)** average (5x5 pixels) spectrum at locations a and b in (C), of dolomite in drill core 131 (976.75–978.20 m depth from left to right). Vertical lines in (B) and (D) highlight the bands used to calculate the Fe^{3+} index and Fe^{2+} index respectively.

410   The Fe^{2+} index highlights the presence of distinct zones of elevated ferrous iron content that appear to crosscut stratigraphy. It
is particularly high above and adjacent to the mineralised dolostone of 131 (Fig. 12). Unlike the hematite alteration, these
zones are not apparent during visual inspection and have thus not been logged/recognized previously. Ferroan calcite or
dolomite (Gaffey, 1986) are identified as minerals that may give rise to the Fe^{2+} absorption feature in the three drill cores.
Based on the observation of Minz (2011) and Lehmann (2012) that Fe-bearing carbonates are closely associated with Cu-
415   sulphide minerals, and the highlighting fluids flow-like path by the Fe^{2+} index (e.g., veins in hole 136 first core associated with
higher copper grade, Appendix 1), it is suggested here that the Fe^{2+} index may provide evidence for hydrothermal alteration.
We use the ferric and ferrous indices as proxies for two different mineral species: iron oxides (hematite) and Fe-bearing
carbonates. These indexes are particularly relevant in this deposit, partly controlled by redox conditions (Speczik & Püttman,
1987; Kucha, 1990; Kopp, 2008). In borehole 131, the Fe^{3+} index indicates the presence of the Rote Fäule at the bottom of the
420   core, while the Fe^{2+} index indicates abundant occurrence of ferrous iron within the sandstones right above this Rote Fäule
alteration zone, that decreases gradually toward shallower level. Contrary to hole 133, alteration in 131, shows gradual change
of the redox state of the sandstones which may be indicative of high permeability and intense rocks-fluid interaction due to
repetitive fluid ascending event. This observation is consistent with the copper grade of these respective drill cores, which is
economical over an interval of 8 metres in 131 vs only 1.5 metres in 133.

425   **4. Discussion**

The results presented in this study indicate that most of the rock-forming and alteration minerals associated with the
Kupferschiefer mineral system can be mapped, at least qualitatively, using extended-range (VNIR-SWIR-MWIR-LWIR)
hyperspectral drill core scanning. This includes the recognition of mineralogical changes that are not visible to the naked eye
but may be important for deciphering the mineralisation history of the Kupferschiefer and vectoring towards mineralisation.
430   While spectral methods worked well on the Zechstein limestone and Grauliegend / Rotliegend sandstones, the Kupferschiefer
sensu stricto proved largely unresponsive to HSI due to its fine grain size and high organic carbon content. Regardless, we

propose several alteration indicators that could help to characterise the Kupferschiefer mineral system, although cannot draw significant conclusions on the ore-forming processes due to the limited number of drill cores included in this study.

Finally, the data collected for this study allow us to compare mineral spectra in both the widely applied VNIR-SWIR and
435   LWIR ranges, and the generally unused MWIR domain. This allows a brief discussion of the potential for MWIR sensors for hyperspectral drill core logging.

4.1. Spectral lithofacies characterisation and alteration mapping

4.1.1. Footwall sandstones

HSI covering the sandstone below the Kupferschiefer characterises the distribution of quartz, sulphate, carbonates and
440   clay/mica minerals. The carbonates feature in the SWIR and the LWIR are only locally present, and indicate the formation of patchy carbonate cement, as was also identified previously using QXRD (Kehrer, 2016). Interestingly, the abundance of carbonate cement appears to be negatively correlated with sulphate abundance (noting that anhydrite cannot be mapped in the sandstones as its emission peak overlaps with the quartz feature). In cores 131 and 133, gypsum appears concentrated along distinct cross-bedding planes, while in 136 it is more widely disseminated. This gypsum does not appear to correlate with the
445   mineralisation, though could provide an important sulphur source during sulphide formation (Oszczepalski, 1999).

Mica and clay minerals are widely distributed within the sandstones, presumably both as diagenetic minerals (such as illite) and also as hydrothermal alteration minerals (e.g. well crystalline kaolinite, Fig. 11). As shown in figure 6, this complicates mapping of the carbonate feature (due to overlapping absorptions in the SWIR range). Differences in the AlOH absorption position suggest a more phengitic cement in hole 133 than 131 and 136, although the potential relationship between this
450   variation and mineralisation cannot be determined from three drill holes. That said, there is a wide body of literature which demonstrates that white-mica composition can be a useful alteration index in many mineral systems (e.g., Laukamp et al., 2011; van Ruitenbeek et al., 2012; Portela et al., 2021).

4.1.2. Footwall alteration

In every Kupferschiefer deposit, the economic Cu-Ag mineralisation is found proximal to a geochemical redox gradient with
455   a highly oxidised region in sharp contact to a still reduced interval (Speczik and Püttman, 1987; Borg et al., 2012). This sudden change in redox state is thought to be the main reason for metal deposition, so identifying and characterising the Rote Fäule is important for exploration and mineral systems analysis. While it is generally easy to identify visually, the VNIR iron indices described in Sect. 3.5. allow quantification of both the intensity of the oxidation and the position and abrupt nature of the redox front.

460   Above this redox front, the pooling (and periodic escape) of the metalliferous fluid below the generally impermeable Kupferschiefer horizon is also thought to control the degree of mineralisation that occurred (Kucha, 1990; Speczik & Püttman, 1987; Kopp, 2008; Borg et al., 2012). Our results show that both of the boreholes containing mineralisation at the base of the Kupferschiefer also showed a distinctive increase in the kaolinite crystallinity index (KI). This observation is consistent with an interpretation of the kaolinite as a hydrothermal alteration mineral and suggests that KI could also be used to track high-
465   temperature fluid flow within the sandstone units. Petrographic observations from Minz (2011) support this interpretation.

4.1.2. Kupferschiefer

The Kupferschiefer itself is difficult to characterise using spectral methods, due to its fine grain size and low reflectivity. This low reflectivity is in part caused by abundant organic matter, which is also thought to have played a fundamental role in metal concentration through catalytic auto oxidation and dehydrogenation (Kucha, 1990). Quantification of the abundance of this
470   organic matter remains a significant challenge using both conventional and spectral techniques. Rahfeld et al. (2018) state that

mineralogical analysis with MLA and XRD is complicated in Kupferschiefer-type deposits because of the extremely fine-grained matrix and the extremely variable Cu-sulphide content within the organic matter-rich material.

Many studies have attempted to map organic carbon in cores and outcrops using hyperspectral methods (e.g., Greenberger et al., 2016), with varying degrees of success. While we tried several of these techniques, we found that the low reflectance of

475 the organic-rich shales made it difficult to confidently identify and map spectral features associated with organic molecules. However, it is possible that more advanced (and properly calibrated) approaches could achieve this, which would be very significant as it would allow quantitative mapping of another key part of the Kupferschiefer mineral system.

4.1.3. Zechstein limestones

Petrographic studies revealed that the Zechstein limestones above the Kupferschiefer have various compositions and textures,

480 due to both diagenetic and hydrothermal processes (Minz, 2011; Lehmann, 2011). This complexity is reflected in the HSI, with carbonate absorption positions suggesting a wide range of carbonate mineralogy and complex spatial variation (e.g. zoned halos around stylolites). Cm-sized anhydrite nodules are also identified in the Zechstein carbonates (Sect. 3.3), although the formation and potential significance of these is unclear. At a larger scale, we note that the Zechstein limestones are dominantly dolomitic in hole 131 and calcitic in 133 and 136, although the significance of this variation (and genesis of the dolomite)

485 remains also unclear.

4.1.4. Hangingwall alteration

After precipitating a Cu-rich mineralisation zone at or immediately below the Kupferschiefer, mineralising fluids appear to have leaked upwards into the Zechstein carbonates to form generally more Pb and Zn-rich ore zones (Rentzsch, 1974; Borg et al., 2012). While our analysis of three drill holes is not sufficient to draw robust conclusions, the iron indices described in Sect.

490 3.5 indicate patchy ferroan calcite and dolomite associated with mineralised zones above the Kupferschiefer. We make the tentative suggestion that these could have formed due to alteration by mineralised fluids in outflow zones above the Kupferschiefer, a process which has been previously inferred at other sediment-hosted hydrothermal systems (Essalhi et al., 2009; Blomme et al., 2017). Observations of cogenetic copper sulphides and iron-enriched carbonate cement within the footwall sandstones by Minz (2011) are consistent with this hypothesis.

495 Unlike the sandstone units, permeability within the Zechstein carbonates appears to have been significantly more variable. Relatively abundant calcite veins and veinlets, often associated with mineralisation, indicate periodically elevated fluid pressures (Fig. 8). It is also interesting that the anastomosing stylolites developed in the Zechstein carbonates have ~5 cm-thick alteration halos enriched in Mg, Si and locally Cu and S (Fig. 8). We suggest that these styolites could counterintuitively represent preferential fluid pathways, focusing mineralising fluids as they ascend above the main mineralised zones. If this

500 were the case, then hyperspectral mapping of these alteration halos could provide an additional proxy for past fluid flow, guiding exploration towards more mineralised areas. The LWIR range spectra appear to be especially sensitive to these halos: the carbonate emission peak at 11300 nm shows a progressive increase towards higher wavelengths in these alteration halos and appears to correlate with regions of higher Pb and Zn grade.

4.2 Full-range HSI for mineral system mapping

505 Exploration typically involves manual drill core logging, followed by metre-scale interval sampling for geochemical analysis. For mineralogical analysis, a discrete sampling scheme is commonly applied where small samples are extracted for detailed analysis using e.g., transmitted light microscopy (Minz, 2011; Lehmann, 2012), MLA or XRD (Kehrer, 2016; Rahfeld et al., 2018). Sample numbers are limited by practical considerations, and selected based on previous (and potentially biased) interpretations of the lithology and styles of mineralisation present.

510   HSI data thus have significant potential to complement this approach by (1) providing continuous mineralogical information (2) objectively capturing relevant geological information for e.g., later re-analysis or re-interpretation, and (3) providing important extra information when selecting sample locations or performing geological logging. These advantages are well documented in other mineral systems (e.g., Tusa et al., 2018), and we suggest that they are equally applicable to Kupferschiefer type sediment-hosted Cu-Ag deposits.

515   Specifically, the results of this pilot study demonstrate that HSI is able to detect and quantify the intensity and gradient of crucial redox boundaries (e.g., Rote Fäule alteration; Fig. 12 and Fig. 13) and potentially important alteration minerals (e.g., high crystallinity kaolinite, Fe-carbonates; Fig. 13). These latter features can be especially difficult to detect visually and show important small-scale variation, preventing accurate characterisation based on averaged or visually guided discontinuous sampling schemes. HSI thus has the potential to fill a significant scale gap and more thoroughly quantify potential alteration

520   indicators in sediment-hosted copper systems, facilitating exploration vectoring and large-scale and mineral system characterisation.

As well as testing HSI methods on Kupferschiefer-type mineralisation, this study deployed a full suite of hyperspectral sensors covering the VNIR-SWIR-MWIR-LWIR range, unlike more established approaches (e.g., data collection limited to the VNIR-SWIR range). Despite containing absorption features associated with many minerals including tourmaline, amphibole, micas,

525   carbonates, quartz and sulphates (Laukamp et al., 2021), the MWIR is a poorly understood spectral range for geological applications. Our results suggest that it is suitable for mapping carbonates and quartz in the various lithologies of the Kupferschiefer and provides important complementary absorption features for SWIR-active minerals that help disentangle complex mixtures. For instance, in the sandstone units, the doublet of carbonate absorption in the MWIR range (Kokaly et al., 2017; Laukamp et al., 2021) was very persistent, while SWIR overtones and LWIR emission peaks were often absent or

530   overprinted by other mineral signatures (e.g., from illite cement). Furthermore, while carbonate absorptions in both the SWIR and MWIR range were found to be sensitive to carbonate composition, the position of the LWIR emission peak appears influenced by a variety of other factors (e.g., Fe-content, Green and Schodlok, 2016; grain size; Zaini et al., 2012; or mixture with sulphates), making it difficult to confidently distinguish calcite from dolomite based on LWIR spectra alone (Fig. 6, 7). This sensitivity of the LWIR does reveal interesting (but more cryptic) variations around e.g., veins and stylolites, and so adds

535   important complementary information.

The MWIR range also proved useful for cross-validating absorption features observed in the SWIR and LWIR ranges, building confidence in our spectral interpretations. For example, quartz emission peaks detected in the LWIR range could be validated against quartz-related absorption features in the MWIR range, allowing confident mapping of quartz even at relatively low concentrations.

540   Finally, it is important to note that care must be taken regarding the storage conditions of the cores. In this study the borehole material was drilled more than 10 years ago and, at certain locations, shows evidence of strong recent oxidation that has nothing to do with the core's oxides content but that can increase the Fe^{3+} index signal. Similarly, we could theoretically distinguish anhydrite from gypsum in fresh cores but suspect that weathering during storage has replaced many anhydrite zones with gypsum. Integration of hyperspectral scanning techniques (and real-time data processing) during exploration would mitigate

545   this issue, while simultaneously providing valuable additional data to enhance conventional logging activities.
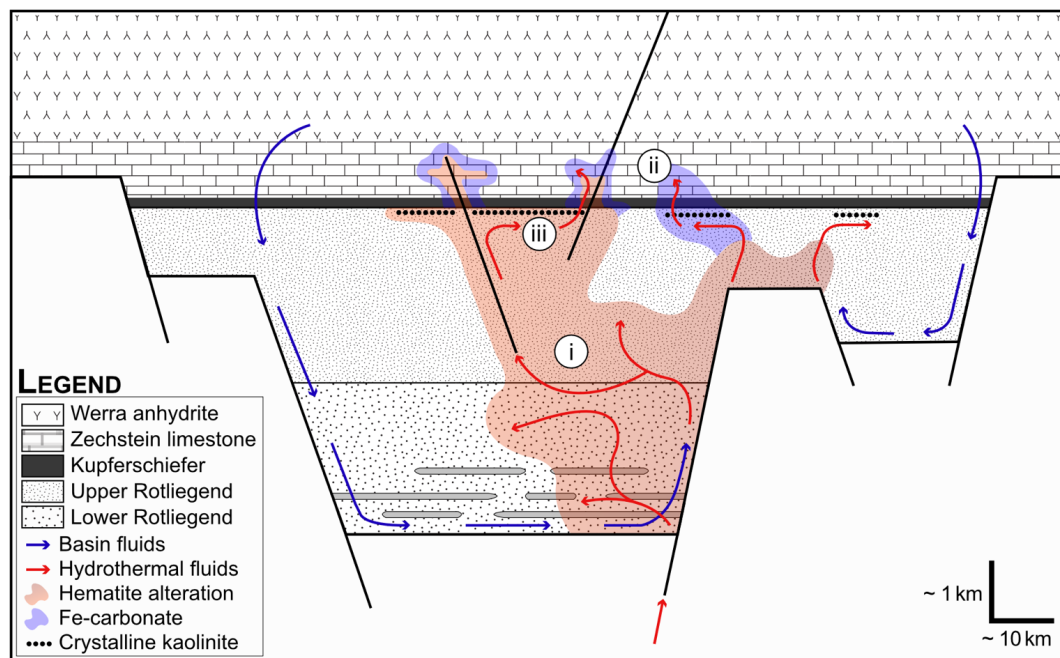
Figure 13. Schematic cross section through the CESB with fluid migration paths and alterations footprint, i.e. hematite alteration ("Rote Fäule"), Fe-carbonate alteration and the occurrence of well crystalline kaolinite. The distribution and relative intensity of these hydrothermal alteration processes are measurable through HSI indexes referred to in this study respectively as, (i) Fe^{3+} index, (ii) Fe^{2+} index and (iii) KI. Grey layers in Lower Rotliegend are thick volcanic piles. (Modified after Borg, 1991 and Borg et al., 2012)

5. Conclusions

This exploratory study demonstrates that full range VNIR-SWIR-MWIR-LWIR hyperspectral drill core scanning can provide important constraints on host rock and alteration mineralogy associated with sediment-hosted copper mineralisation. Iron indices sensitive to the redox state map the redox front thought to have triggered metal deposition in the Kupferschiefer, and possibly also track the inflow and outlflow paths of hydrothermal fluids on a local and regional scale. The kaolinite crystallinity index supports previous work indicating the formation of hydrothermal kaolinite in physical traps below the Kupferschiefer, while alteration halos around stylolites provide evidence for localised fluid flow in the overlying Zechstein limestone. While analyses of a large number of drill holes is needed to place these observations in the larger mineral system, we suggest that full range hyperspectral drill core scanning could provide a useful tool for exploration companies searching for sedimentary hosted copper deposits. This method enhances geological logging, enables data-driven sampling strategies and allows objective and consistent measures of lithology or alteration for input into, e.g., three-dimensional modelling workflows (e.g., De La Rosa et al., 2022).

Code/Data availability

The processed data that support the findings of this study are available from the corresponding author upon reasonable request.

Author contribution

Example: LG participated in data acquisition and conducted the spectral analysis, and was the main contributor of the original manuscript. MK co-developed the concept, helped obtain the funding and material for this project, and assisted with figure preparation and contributed with writing/editing of the manuscript. ST developed the software, guided the experiments and provided assistance in the spectral analysis and its validation. He also substantially contributed to writing/editing of the

manuscript. ADLR performed/supervised the µXRF analytical work for validation and helped visualize these data. RG helped

edit the manuscript, contributed to funding acquisition, project administration and supervision as well as provision of core

575 material and instrumentation. JG co-defined the concept and research goals of this study and helped acquire the funding. He

provided guidance in the interpretation of the data and contributed greatly to the original manuscript preparation.

Competing interests

The authors declare that they have no conflict of interest.

580 **Acknowledgements**

The authors thank KSL Kupferschiefer Lausitz GmbH (Spremberg, Germany) and its parent company Minera S.A. for

generously providing funding, drill core material as well as analytical data. We are grateful to Yuleika Madriz and Erik

Hermann for their help with hyperspectral data acquisition, to Sandra Lorentz for help with pre-processing, and to Laura Tusa

for her input regarding spectral interpretation.

585 **References**

Agricola, G., Hoover, H., Hoover, L.H.: De re metallica. Dover Publications, New York, United States of America, 1950.

Bechtel, A., Sun, Y., Püttmann, W., Hoernes, S., Hoefs, J.: Isotopic evidence for multi-stage base metal enrichment in the Kupferschiefer from the Sangerhausen Basin, Germany, Chemical Geology, 176, 31–49, 10.1016/S0009-2541(00)00336-3, 2001.

590 Bedini, E.: The use of hyperspectral remote sensing for mineral exploration: a review, Journal of Hyperspectral Remote Sensing, 7, 189–211, https://doi.org/10.29150/jhrs.v7.4.p189-211, 2017.

Blomme, K., Fowler, S. J., Bachaud, P., Nader, F. H., Michel, A. and Swennen, R.: Ferroan Dolomitization by Seawater Interaction with Mafic Igneous Dikes and Carbonate Host Rock at the Latemar Platform, Dolomites, Italy: Numerical Modeling of Spatial, Temporal, and Temperature Data, Geofluids, 2017, 1-14. doi:10.1155/2017/6590672, 2017.

595 Borg, G.: The significance of Rotliegend volcanics for the metal provinces of the Kupferschiefer basin, Zentralblatt für Geologie und Paläontologie, 1991, 4/1, 929−943, 1991.

Borg, G., Piestrzyński, A., Barchmann Heinz, G.: An overview of the European Kupferschiefer deposits, Economic Geology Special Publication, 455–486, 2012.

Burns, R.G.: Mineralogical applications of crystal field theory. Cambridge University Press, New York, United States of 600 America, (551 p.), 1993.

Coward, M. P.: Structural and Tectonic Setting of the Permo-Triassic Basins of Northwest Europe, Geological Society, London, Special Publication, 91, 7–39, doi:10.1144/GSL.SP.1995.091.01.02, 1995.

Cudahy, T., Jones, M., Thomas, M., Laukamp, C., Caccetta, M., Hewson, R., Rodger, A.,Verrall, M.: Next Generation Mineral Mapping: Queensland airborne HyMap and satellite ASTER surveys 2006-2008, doi:10.13140/RG.2.1.2828.1844, 605 2008.

De La Rosa, R., Khodadadzadeh M., Tusa, L., Kirsch, M., Gisbert, G., Tornos, F., Tolosana-Delgado R., Gloaguen, R.: Mineral quantification at deposit scale using drill-core hyperspectral data: A case study in the Iberian Pyrite Belt, Ore Geology Reviews, 139, Part B, 104514, doi:10.1016/j.oregeorev.2021.104514, 2021.

De La Rosa, R., Tolosana-Delgado, R., Kirsch, M., Gloaguen, R.: Automated Multi-Scale and Multivariate Geological 610 Logging from Drill-Core Hyperspectral Data, Remote Sensing, 14, 2676, doi:10.3390/rs14112676, 2022.

Essalhi, M., Sizaret, S., Barbanson, L., Chen, Y., Branquet, Y., Panis, D., Camps, P., Rochette, P., Canals, A.: Track of fluid paleocirculation in dolomite host rock at regional scale by the Anisotropy of Magnetic Susceptibility (AMS): An example from Aptian carbonates of La Florida, Northern Spain, Earth and Planetary Science Letters, 277, 501-513, doi:10.1016/j.epsl.2008.11.011, 2009.

615 Gaffey, S.J.: Spectral Reflectance of Carbonate Minerals in the Visible and near Infrared (0.35–2.55 Microns); Calcite, Aragonite, and Dolomite, Am. Miner., 71, 151–162, 1986.

Glennie, K. W., Buller, A. T.: The Permian Weissliegend of NW Europe: The partial deformation of aeolian dune sands caused by the Zechstein transgression, Sedimentary Geology, 35, 43–81, doi:10.1016/0037-0738(83)90069-6, 1983.

GMEX - Spectral interpretation field manual, 3rd edition. AuSpec International Ltd., v. I, II, III, 2008.

620 Green, D., Schodlok, M.: Characterisation of carbonate minerals from hyperspectral TIR scanning using features at 14 000 and 11 300 nm, Australian Journal of Earth Sciences, 1–7, doi:10.1080/08120099.2016.1225601, 2016.

Greenberger, R., Ehlmann, B., Jewell, P., Birgenheier, L., Green, R.: Detection of Organic-Rich Oil Shales of the Green River Formation, Utah, with Ground-Based Imaging Spectroscopy, doi:10.1109/WHISPERS.2016.8071807, 2016.

Hancock, N. J.; Taylor, A. M.: Clay mineral diagenesis and oil migration in the Middle Jurassic Brent Sand Formation, 625 Journal of the Geological Society, 135, 69–72, doi:10.1144/gsjgs.135.1.0069, 1978.

Harraden, C. L., Mcnulty, B. A., Gregory, M. J., Lang, J. R.: Shortwave Infrared Spectral Analysis of Hydrothermal Alteration Associated with the Pebble Porphyry Copper-Gold Molybdenum Deposit, Iliamna, Alaska, Society of Economic Geologists, Inc., 108, 483–494, doi:10.2113/econgeo.108.3.483, 2013.

Jébrak, M. and Marcoux, É.: Géologie des ressources minérales. Avec la collaboration de Michelle Laithier (illustrations). 630 Ministère des ressources naturelles et de la faune, Québec, Canada, 2008.

Jones, S., Herrmann, W., Bruce, G.: Short Wavelength Infrared Spectral Characteristics of the HW Horizon: Implications for Exploration in the Myra Falls Volcanic-Hosted Massive Sulfide Camp, Vancouver Island, British Columbia, Canada, Society of Economic Geologists, Inc., 100, 273–294, doi:10.2113/gsecongeo.100.2.273, 2005.

Kehrer, Christin: Geometallurgical assessment of the Kupferschiefer-type base metal deposit Spremberg-Graustein, Lusatia, 635 Germany. PhD. thesis, Technical University Bergakademie, Freiberg, Germany, 2016.

Kokaly, R. F., Clark, R. N., Hoefen, T. M., Livo, K. E., Pearson, N. C., Swayze, G. A. et al.: USGS Spectral Library Version 7. U.S. Geological Survey Data Series, 1035, doi:10.3133/ds1035, 2017.

Kopp, J., Simon, A., Göthel, M.,: Die Kupfer-Lagerstätte Spremberg-Graustein in Südbrandenburg: Brandenburgische Geowissenschaftliche Beiträge, 640 https://gruendungsnetz.brandenburg.de/sixcms/media.php/4055ver%c3%b6ffkoppsimong%c3%b6thelsprembergnk.pdf, 2006.

Kopp, J., Hermann, S., Hoding, T., Andreas, S., Bernd, U.: The Copper-Silver Deposit Spremberg-Graustein (Lusatia. F. R. Germany) – (Enrichment of non-ferrous metals at the Zechstein-base between Spremberg and Weißwasser), 2008.

Kopp, J., Spieth, V., Höding, T.: The Return of the Copper Mining in Germany (Die Rückkehr des Kupferschieferbergbaus 645 nach Deutschland), Glückauf, 146, 353–363, 2010.

Kopp, J. C., Spieth, V., Bernhardt, H.-J., (Aucune): Precious metals and selenides mineralisation in the copper-silver deposit Spremberg-Graustein, Niederlausitz, SE-Germany, Zeitschrift der Deutschen Gesellschaft für Geowissenschaften, 163, 361–384, doi:10.1127/1860-1804/2012/0163-0361, 2012.

Kucha, H.: Geochemistry of the Kupferschiefer, Poland, Geologische Rundschau, 79, 387–399, doi:10.1007/BF01830634, 650 1990.

Laukamp, C., Cudahy, T., Thomas, M., Jones, M., Cleverley, J. S., Oliver, N. H. S.: Hydrothermal mineral alteration patterns in the Mount Isa Inlier revealed by airborne hyperspectral data, Australian Journal of Earth Sciences, 58, 917–936, doi:10.1080/08120099.2011.571287, 2011.

Laukamp, C., Rodger, A., LeGras, M., Lampinen, H., Lau, I. C., Pejcic, B. et al.: Mineral physicochemistry underlying 655 feature-based extraction of mineral abundance and composition from shortwave, mid and thermal infrared reflectance spectra, Minerals, 11, 347, doi:10.3390/min11040347, 2021.

Lauri, L.: Identification and quantification of primary CRM resources in Europe. GTK, 2018.

Leguérinel M., Gleuher, M.: Le cuivre: revue de l'offre mondiale en 2019. Rapport final. BRGM/RP-69037-FR, 86p., 62 fig., 10 tab. BRGM, 2019.

660 Lehmann, C.: Cement stratigraphy of mineralized Zechstein carbonate rocks of the Cu-Ag deposit Spremberg-Graustein, Lusatia, Germany. B.Sc. thesis, Technical University Bergakademie, Freiberg, Germany, 2012.

Mantovani, M., Escudero, A., Becerro, A. I.: Effect of pressure on kaolinite illitization, Applied Clay Science, 50, 342–347, doi:10.1016/j.clay.2010.08.024, 2010.

Minz, F.: Cement Stratigraphy of the Siliciclastic Sedimentary Footwall Rocks below the Kupferschiefer from the Cu-Ag 665 Deposit Spremberg, Lusatia, Germany. M.Sc. Technical University Bergakademie, Freiberg, Germany, 2011.

McKie, T.: Paleogeographic Evolution of Latest Permian and Triassic Salt Basins in Northwest Europe, in: Permo-Triassic Salt Provinces of Europe, North Africa and the Atlantic Margins, edited by: Soto, J., Flinch, J., Tari, G., Elsevier, 159–173, 2017.

670 Oszczepalski, S., Nowak, G. J., Bechtel, A., Zák, K.: Evidence of oxidation of the Kupferschiefer in the Lubin-Sieroszowice deposit, Poland: implications for Cu-Ag and Au-Pt-Pd mineralisation, Geological Quarterly, 46, 1–23, 2002.

Oszczepalski, S., Speczik, S., Zieliński, K., Chmielewski, A. The Kupferschiefer Deposits and Prospects in SW Poland: Past, Present and Future, Minerals, 9, 592, doi:10.3390/min9100592, 2019.

Park, C., Kim, N., Choi, S.-J., Song, Y.: Mg-Phengite in Carbonate Rock Syngenetically Formed from Hydrothermal Fluid: Micro-Textural Evidence and Mineral Chemistry, Minerals, 10, 668, doi:10.3390/min10080668, 2020.

675 Portela, B., Sepp, M., van Ruitenbeek, F., Christoph Hecker, C., Dilles, J.H.: Using hyperspectral imagery for identification of pyrophyllite-muscovite intergrowths and alunite in the shallow epithermal environment of the Yerington porphyry copper district, Ore Geology Reviews, 131, doi:10.1016/j.oregeorev.2021.104012, 2021.

Rahfeld, A., Kleeberg, R., Möckel, R., Gutzmer, J.: Quantitative mineralogical analysis of European Kupferschiefer ore. In : Minerals Engineering, 115, 21–32, doi:10.1016/j.mineng.2017.10.007, 2018.

680 Rentzsch, J.: The Kupferschiefer in comparison with the deposits of the Zambian Copperbelt, Annales de la Société géologique de Belgique, Special Publications, Gisements stratiformes et provinces cuprifères - Centenaire de la Société Géologique de Belgique, 1974, 395-418, https://popups.uliege.be/0037-9395/index.php?id=3595, 1974.

Schmidt Mumm, A.; Wolfgramm, M.: Fluid systems and mineralization in the north German and Polish basin, Geofluids, 4, 315–328, doi:10.1111/j.1468-8123.2004.00090.x, 2004.

685 Schmidt, F. P.: Alteration zones around Kupferschiefer-type base metal mineralization in West Germany, Mineralium Deposita, 22, doi:10.1007/BF00206606, 1987.

Speczik, S., Püttman, W.: Origin of Kupferschiefer mineralisation as suggested by coal petrology and organic geochemical studies, Acta Geologica Polonica, 37, 1987.

Spieth, V.: Zechstein Kupferschiefer at Spremberg and Related Sites : Hot Hydrothermal Origin of the Polymetallic Cu-Ag-
690 Au Deposit. PhD. thesis, University of Stuttgart, doi:10.18419/opus-10530, 2019.

Stoll, Michael: Deportment of critical metals and process mineralogy of Kupferschiefer ores from the Polkowice-Sieroszowice mine, SW Poland. B.Sc. thesis, Faculty of Geology and Petrology, Institute of Mineralogy, Technical University Bergakademie, Freiberg, Germany, 2014.

Sun, Y. Z., Püttmann, W.: Metal accumulation during and after deposition of the Kupferschiefer from the Sangerhausen
695 Basin, Germany, Appl. Geochem. 12, 577–592, doi:10.1016/S0883-2927(97)00015-2, 1997.

Tappert, M. C., Rivard, B., Tappert, R., Feng, J.: Using Reflectance Spectroscopy to Estimate the Orientation of Quartz Crystals in Rocks, The Canadian Mineralogist, 51, 405-413, doi:10.3749/canmin.51.3.405, 2013.

Thiele, S., Lorenz, S., Kirsch, M., Contreras Acosta, C., Tusa, L., Hermann, E., Mockel, R., Gloaguen, R.: Multi-Scale, Multi-Sensor Data Integration for Automated 3-D Geological Mapping, Ore Geology Reviews, 136,
700 doi:10.1016/j.oregeorev.2021.104252, 2021.

Thompson, A. J. B., Phoebe, L. H., Audrey, J. R.: Alteration Mapping in Exploration: Application of Short-Wave Infrared (SWIR) Spectroscopy, Society of Economic Geologists, Newsletter, 39, 1–27, doi:10.5382/SEGnews.1999-39.fea, 1999.

Tusa, L., Andreani, L., Pohl, E., Contreras, I. C., Khodadadzadeh, M.i, Gloaguen, R., Gutzmer, J.: Extraction of Structural and Mineralogical Features from Hyperspectral Drill-Core Scans, IEEE IGARSS 2018 - 2018 IEEE International
705 Geoscience and Remote Sensing Symposium - IEEE International Geoscience and Remote Sensing Symposium, Valencia, 4070–4073, doi:10.1109/IGARSS.2018.8517786, 2018.

Tusa, L., Khodadadzadeh, M., Contreras, C., Rafiezadeh Shahi, K., Fuchs, M., Gloaguen, R., Gutzmer, J.: Drill-Core Mineral Abundance Estimation Using Hyperspectral and High-Resolution Mineralogical Data, Remote Sensing, 12.,1218, doi:10.3390/rs12071218, 2020.

710 Van der Meer, F.: Analysis of spectral absorption features in hyperspectral imagery. Int. J. Appl. Earth Obs. Geoinf., 5, 55–68, doi:10.1016/j.jag.2003.09.001, 2004.

Van Ruitenbeek, F., Bakker, W. H., van der Werff, H., Zegers, T. E., Oosthoek, J. H., Omer, Z. A., Marsh, S., van der Meer, F. D.: Mapping the wavelength position of deepest absorption features to explore mineral diversity in hyperspectral images, Planet. Space Sci., 101, 108–117, doi:10.1016/j.pss.2014.06.009, 2014.

715 Van Ruitenbeek, F., Cudahy, T.-J., Van der Meer, F.-D., Hale, M.: Characterization of the hydrothermal systems associated with Archean VMS-mineralization at Panorama, Western Australia, using hyperspectral, geochemical and geothermometric data, Ore Geology Reviews, 45, 33-46, doi:10.1016/j.oregeorev.2011.07.001, 2012.

Wodzicki, A., and A. Piestrzyński.: An Ore Genetic Model for the Lubin - Sieroszowice Mining District, Poland, Mineralium Deposita, 29, 30-43, doi:10.1007/BF03326394, 1994.

720   Zaini, N., Meer, F., van der Werff, H.: Effect of Grain Size and Mineral Mixing on Carbonate Absorption Features in the SWIR and TIR Wavelength Regions. Remote Sensing, 4, doi:10.3390/rs4040987, 2012.

Appendices
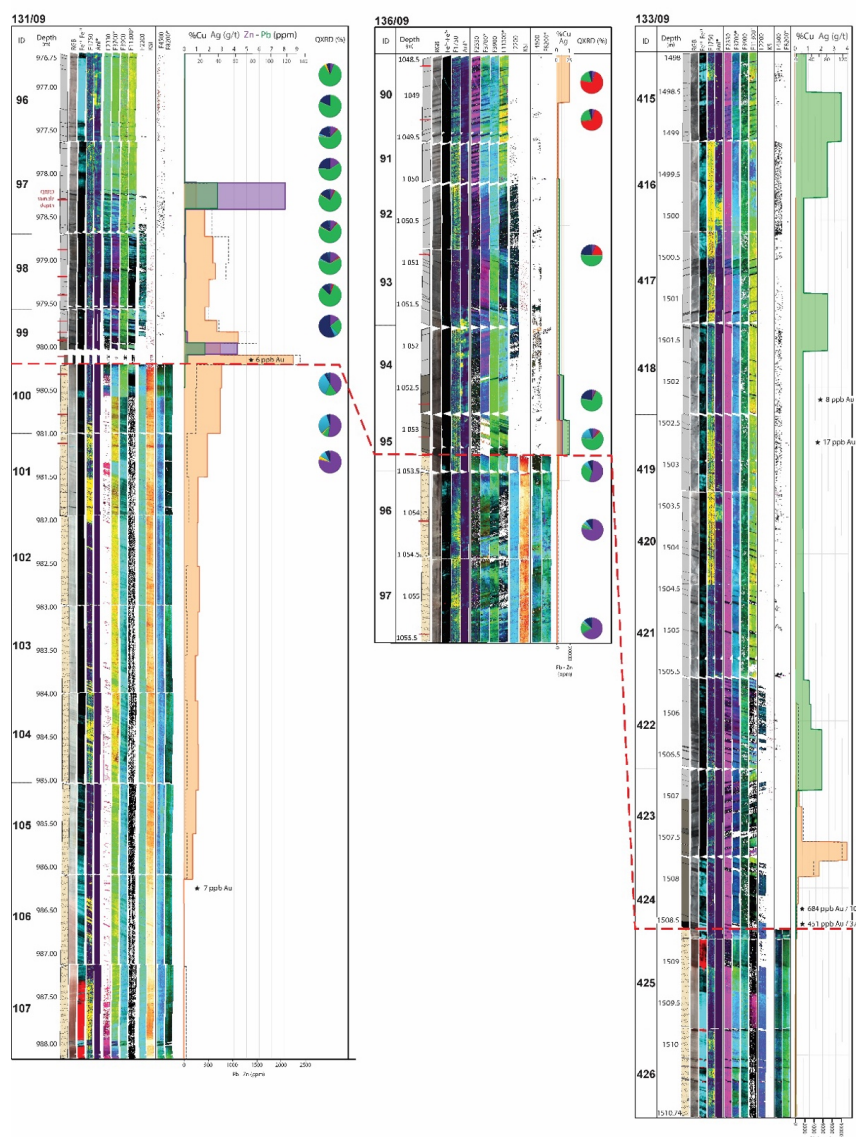
Appendix 1. Spectral features maps and copper grade of the three drill core sections.

LEGEND
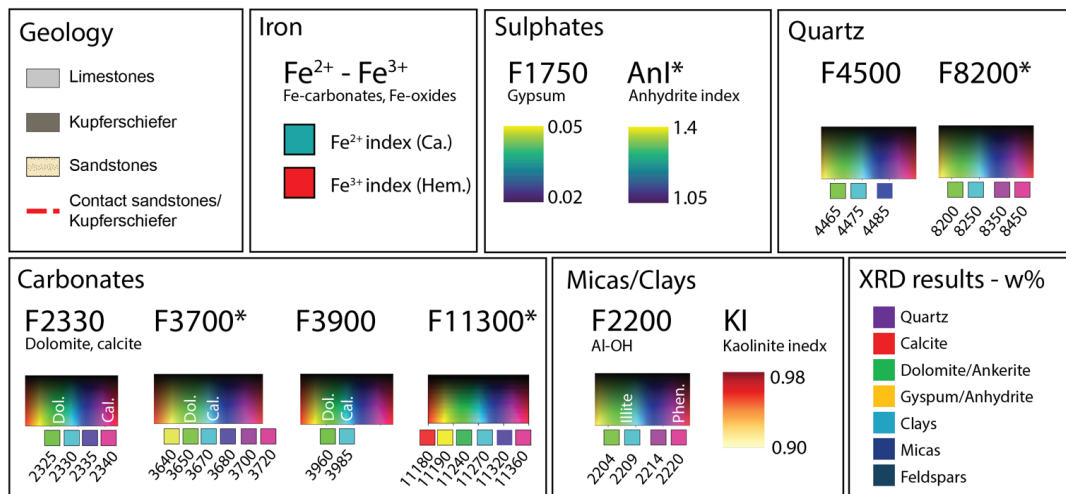
* emission peak

730   **Appendix 2. Legend of lithologic log, HSI maps and QXRD results of Appendix 1.**